



ORIGINAL RESEARCH ARTICLE

Inhibition of NOX1 Mitigates Blood Pressure Increases in Elastin Insufficiency

Angela Troia^{1,#}, Russell H. Knutsen ^{1,#}, Carmen M. Halabi², Daniela Malide¹, Zu Xi Yu¹, Amanda Wardlaw-Pickett¹, Elise K. Kronquist¹, Kit Man Tsang¹, Attila Kovacs³, Robert P. Mecham⁴, Beth A. Kozel ^{1,*}

¹National Heart Lung and Blood Institute, National Institutes of Health, Bethesda, MD, USA, ²Department of Pediatrics, Washington University School of Medicine, St. Louis, MO, USA, ³Department of Internal Medicine, Cardiovascular Division, Washington University School of Medicine, St. Louis, MO, USA, ⁴Department of Cell Biology and Physiology, Washington University School of Medicine, St. Louis, MO, USA

#Angela Troia and Russell H. Knutsen are authors who contributed equally.

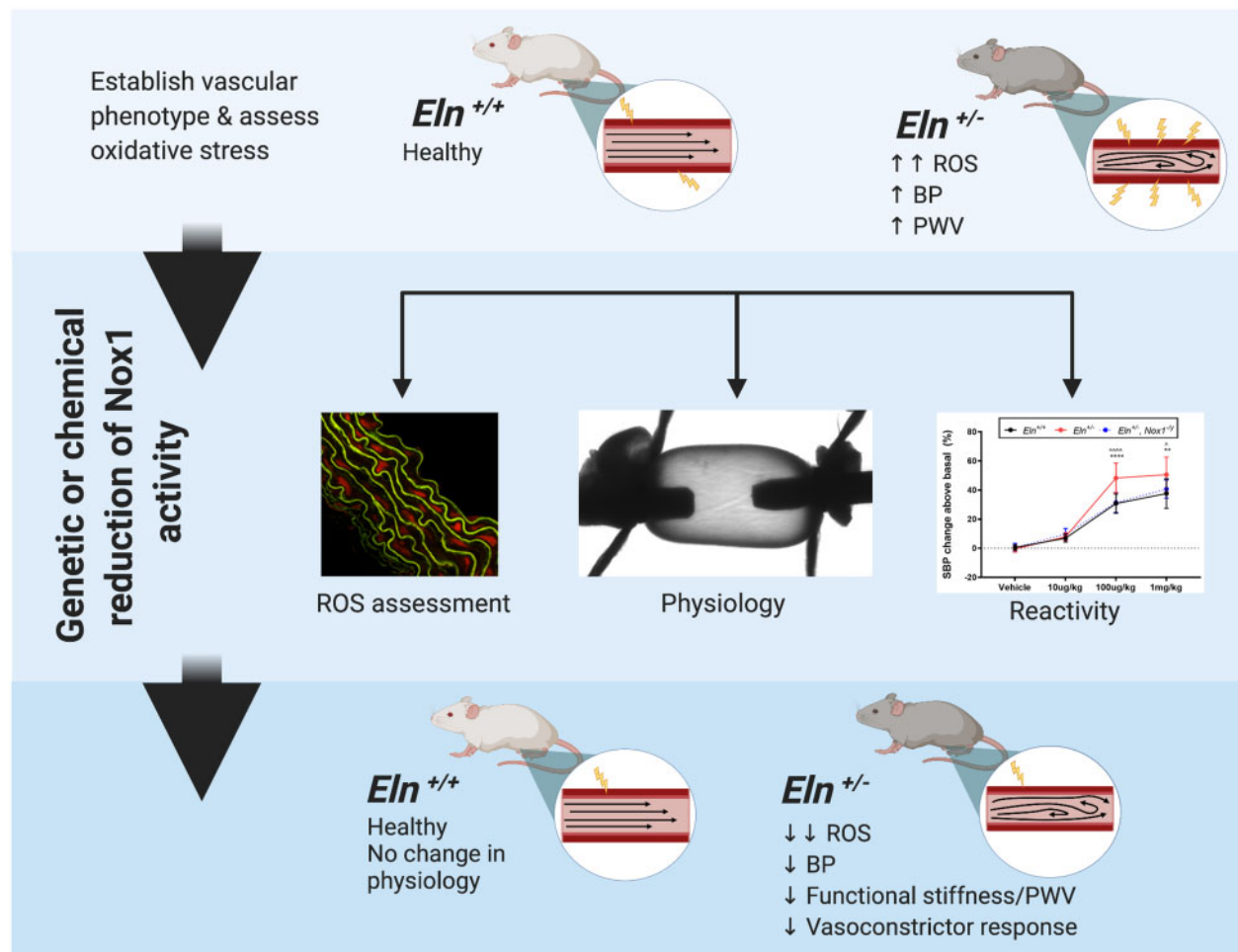
*Address correspondence to B.A.K. (e-mail: Beth.Kozel@nih.gov)

Abstract

Elastin (ELN) insufficiency leads to the cardiovascular hallmarks of the contiguous gene deletion disorder, Williams–Beuren syndrome, including hypertension and vascular stiffness. Previous studies showed that Williams–Beuren syndrome deletions, which extended to include the *NCF1* gene, were associated with lower blood pressure (BP) and reduced vascular stiffness. *NCF1* encodes for p47phox, the regulatory component of the NOX1 NADPH oxidase complex that generates reactive oxygen species (ROS) in the vascular wall. Dihydroethidium and 8-hydroxyguanosine staining of mouse aortas confirmed that *Eln* heterozygotes (*Eln*^{+/-}) had greater ROS levels than the wild-types (*Eln*^{+/+}), a finding that was negated in vessels cultured without hemodynamic stressors. To analyze the Nox effect on ELN insufficiency, we used both genetic and chemical manipulations. Both *Ncf1* haploinsufficiency (*Ncf1*^{+/-}) and *Nox1* insufficiency (*Nox1*^{-/-}) decreased oxidative stress and systolic BP in *Eln*^{+/-} without modifying vascular structure. Chronic treatment with apocynin, a p47phox inhibitor, lowered systolic BP in *Eln*^{+/-}, but had no impact on *Eln*^{+/+} controls. In vivo dosing with phenylephrine (PE) produced an augmented BP response in *Eln*^{+/-} relative to *Eln*^{+/+}, and genetic modifications or drug-based interventions that lower *Nox1* expression reduced the hypercontractile response to PE in *Eln*^{+/-} mice to *Eln*^{+/+} levels. These results indicate that the mechanical and structural differences caused by ELN insufficiency leading to oscillatory flow can perpetuate oxidative stress conditions, which are linked to hypertension, and that by lowering the *Nox1*-mediated capacity for vascular ROS production, BP differences can be normalized.

Submitted: 1 January 2021; Revised: 6 March 2021; Accepted: 9 March 2021

Published by Oxford University Press on behalf of American Physiological Society 2021. This work is written by US Government employees and is in the public domain in the US.



Key words: elastin; Nox1; Nox2; reactive oxygen species; Williams syndrome; NADPH oxidase; hypertension; oscillatory flow

Introduction

Vascular reactive oxygen species (ROS) are signaling molecules that play an important physiological role in controlling endothelial function and vascular tone, factors that can affect vessel mechanics associated with arterial stiffening.^{1–4} Arterial stiffness is a hallmark of hypertension, and a common feature of aging.⁵ People with Williams–Beuren syndrome (Williams syndrome, WS) have a congenital vasculopathy as a result of a deletion of 25–27 genes from chromosome 7, including the elastin (ELN) gene. ELN encodes for the extracellular matrix protein, ELN, an important component of the vascular wall that provides recoil to elastic vessels.⁶ Arteries with reduced ELN content are less compliant and develop structural modifications that include increased numbers of smooth muscle and elastic lamellae. Consequently, individuals with ELN insufficiency have developmentally, rather than environmentally, induced vascular stiffness.⁷ They also have anatomical differences in branching and arterial tortuosity. Recent work by our group and others revealed that deletions, which reduce copy number for NCF1, are associated with lower risk of hypertension than those deletions in which the individual retained both copies.^{7,8}

Remarkably, an unbiased genetic screen for modifiers of ELN-mediated vascular disease using quantitative trait locus analysis in more than 600 *Eln*^{+/-} mice also suggested *Ncf1* as a likely modifier.⁹

The *Ncf1* gene encodes for p47phox, the regulatory subunit of NOX1 and NOX2 NADPH oxidase complexes that generate ROS in the vascular wall and have been implicated in hypertension and vascular disease. Each NOX complex is made up of 6 subunits including a catalytic domain Nox1 (Nox1, gp91-2) in the NOX1 complex and Nox2 (Cybb, gb91phox) in the NOX2 complex.^{10,11} These complexes catalyze the conversion of NADPH and oxygen to NADP⁻, superoxide, and hydrogen. Nox1 and Nox2 are differentially expressed and vary in ROS-generating activity. The NOX1 complex is produced by endothelial and smooth muscle cells (SMCs), whereas NOX2 is made by endothelial cells, adventitial fibroblasts, and inflammatory cells.¹² ELN insufficiency outcomes are not thought to be primarily mediated by inflammation, making a NOX1-mediated mechanism more attractive. Reduction in blood pressure (BP) has been seen for Nox1^{-/-} mice in angiotensin infusion-induced hypertension models; however, the Nox1 complex has not been studied in genetic, or specifically structural, models of hypertension. *Eln*^{+/-}

mice have stiff, tortuous, and narrow vasculature^{10,13–16} and recapitulate much of the human disease of WS, manifesting hypertension, arterial stiffness, and having increased numbers of elastic lamellae in their arteries.¹ Given that the WS vascular phenotype appears to be modified by *NCF1*, it is important to understand how this complex, and the ROS it produces, modifies disease severity. Determining whether the NOX1 complex can be implicated in the vascular pathology associated with WS and *Eln* insufficiency may guide therapy for patients with this condition.

Materials and Methods

Study Approval and Animal Lines

Experiments were approved by the animal studies committees at Washington University School of Medicine or the National Heart, Lung and Blood Institute of the National Institutes of Health. All animals studied in a particular experiment were housed similarly in accordance with institutional guidelines. Littermates were used when available. Not all studies were performed on all animals.

Eln^{+/-} mice were first described by Li et al.¹⁵ This animal was additionally backcrossed into C57Bl6/J, and Single nucleotide polymorphism (SNP) genotyping was performed to assure a majority C57Bl6/J background.⁹ To generate the double mutant lines, the *Eln*^{+/-} was crossed to *Ncf1*^{+/-} (B6(Cg)-*Ncf1m1J*/J; JAX #004742), *Nox1*^{-/-} (B6.129X1-*Nox1tm1Kkr*/J; JAX #018787), or *Nox2*^{-/-} (*Nox2* B6.129S-Cybbtm1Din/J; JAX #002365). Because *Nox1* and *Nox2* are on the X chromosome, all studies were performed in male mice to avoid the complex impact of lyonization in heterozygous females. Previous studies in *Eln*^{+/-} mice showed no difference in phenotypes between males and females, except in aged mice.¹⁷

Aortic Flow Visualization

To view flow in the ascending aorta, *Eln*^{+/+} and *Eln*^{+/-} mice were anesthetized with isoflurane anesthesia (1.5%) and the aortic arch was imaged with high-resolution, high-frame rate 2D images from the right-sided superior parasternal view using a 35 MHz ultrasound transducer. Electrocardiogram (ECG)-triggered image reconstruction at 1000 frames/s using ECG-gated KiloHertz Visualization¹⁸ image acquisition mode allows for increased temporal and spatial resolution imaging. By averaging multiple cardiac cycles, typical B-mode frame rates are increased from approximately 200 to up to 10 000 frames/s. At this high spatial and temporal resolution, the technique allows visualization of blood flow pattern.

In Situ Detection of Vascular O₂— Production: Dihydroethidium Assay

The oxidative fluorescent dye, dihydroethidium (DHE, D11347, Invitrogen, Eugene, OR) was used to evaluate production of O₂⁻ in situ. Matched groups of *Eln*^{+/+} and *Eln*^{+/-} mice were sacrificed on the same day via CO₂ inhalation, and aortic tissue was immediately dissected out and frozen in optimal cutting temperature compound (OCT, Tissue-Plus O.C.T. Compound, 23-730-571, Fisher, Houston, TX). Because of the volatile nature of the compounds used, samples were processed only 2 at a time (1 *Eln*^{+/+} and 1 *Eln*^{+/-}). Within 90 min of euthanasia, 12 μm sections were cut from both blocks, placed on separate glass slides, and incubated with 10 μM DHE (10 μM) in phosphate-buffered saline (PBS, Mediatech Inc, Manassas) in a light protected, humidified

chamber for 30 min, as previously described.^{19–21} After treatment, slides were washed with 1× PBS, then mounted with 4,6-diamidino-2-phenylindole (DAPI) mounting medium (Vectashield, Burlingame, H-1200) and cover slipped. Slides were then imaged using a Zeiss 780 inverted confocal microscope with the following imaging configurations: DAPI (Ex:Em= 405/397–440 nm), DHE (Ex:Em= 488/579–659 nm),^{22,23} and *Eln* (by autofluorescence Ex:Em= 488/490–562 nm) (Supplemental Figures S1A–C, respectively). Additional *Eln*^{+/+} and *Eln*^{+/-} pairs were subsequently processed for replication. Images shown were optimized identically in PowerPoint for display, but these changes were not used during the calculation of fluorescence. To analyze quantitatively DHE fluorescence intensity, we used Imaris software v 9.5 (Bitplane, Zurich, Switzerland). The DAPI channel was used to segment the nuclei as “surface” objects (Supplemental Figure S1D). These surfaces were used as positive selection masks to extract fluorescence intensity values (mean intensity) in the DHE channel underlying each masked region (nuclei) (Supplemental Figure S1E), allowing us to calculate the intensity per nucleus value and avoid any autofluorescence from the nearby elastic lamina. The intensity per nucleus was then averaged across the sample. Nuclei in the adventitia were excluded in our measurements by using the external elastic lamellae as a boundary for the measure. Three images per sample were quantified and the average DHE fluorescence intensity was calculated. The number and area of the nuclei were determined to ensure the number and area were comparable between different samples and did not influence the mean fluorescence intensity results (Supplemental Figure S1F).

Organ Culture

Mice were sacrificed as above. Ascending aortas (*Eln*^{+/+} and *Eln*^{+/-}) were dissected free, rinsed with PBS, and cut into 2 pieces using surgical scissors. The 2 halves were cultured for 16 h at 37°C, 5% CO₂ in Dulbecco's Modified Eagle Medium (DMEM, Gibco 10566032) supplemented with 10% fetal bovine serum (Cytiva SH30071.03HI), 1× nonessential amino acid (Gibco 11140050), and 1 mM sodium pyruvate (Gibco 11360070). Before evaluation with DHE as defined above, 1 of the 2 pieces of aorta was treated with a ROS inducer Antimycin A (AMA 20 μM, Abcam, San Francisco, ab141904) for 60 min at 37°C in DMEM media in a CO₂ hood to confirm viability and the retained ability to produce ROS after culture. After completion of treatments, aortas were flash frozen in OCT, sectioned, and stained with DHE as described above. Fresh (real-time) aortas were processed on the day of DHE treatment for comparison to the organ culture samples. DHE was quantified as above.

Vascular Ex vivo Viability

Mice were sacrificed as above. Aortas were then flushed with physiologic salt solution (PSS; NaCl 130 mM, KCl 4.7 mM, KH₂PO₄ 1.18 mM, MgSO₄·7H₂O 1.17 mM, NaHCO₃ 14.9 mM, dextrose 5.5 mM, EDTA 0.026 mM, CaCl₂ 1.6 mM, pH 7.4—all components from Sigma Aldrich, St Louis, MO), via the left ventricle, and a single 2-mm segment of ascending aorta was isolated. Aortic segments were either immediately mounted on a wire myograph (Model 620M, Danish Myotechnology, Denmark) in cold PSS and equilibrated at 37°C for 20 min with continuous oxygenation (95% O₂, 5% CO₂) or placed in tissue culture media for 16 h (as in the organ culture section above) and mounted on the myograph after the no-flow period. Viability was confirmed with potassium PSS (KPSS; NaCl 74.7 mM, KCl

60 mM, KH_2PO_4 1.18 mM, $\text{MgSO}_4 \cdot 7\text{H}_2\text{O}$ 1.17 mM, NaHCO_3 14.9 mM, dextrose 5.5 mM, EDTA 0.026 mM, CaCl_2 1.6 mM), after which vessels were then washed with PSS to return to baseline, and appropriate smooth muscle and endothelial cell function were confirmed with administration of phenylephrine (PE, 10^{-4} M in PSS; Sigma Aldrich P6126) followed by acetylcholine (ACh, 10^{-4} M in PSS; Sigma Aldrich A2661) (data not shown). Vessels were, again, washed with PSS and allowed to rest for 20 min and a final dose of KPSS was added to elicit a maximal contraction. After resting again, 3 increasing doses of PE (10^{-4} M, 10^{-3} M, and 10^{-2} M) were administered at 10-min intervals and the vessel contractile force was assessed. Vessels cultured in DMEM overnight were subsequently subjected to the same reactivity protocol to determine whether culture had altered vessel viability/function. Data are reported as fraction of maximal contraction, with the highest dose of PE eliciting the highest contraction (1) and lower doses eliciting a portion of the final contraction.

Chronic Apocynin Treatment

At 4–6 weeks of age, male $\text{Eln}^{+/+}$ and $\text{Eln}^{+/-}$ mice were subcutaneously implanted with ALZET microosmotic pumps (model 1004; DURECT, Cupertino, CA) as previously described.⁶ Pumps delivered a continuous dose of 50% dimethyl sulfoxide (DMSO) in water, or 3/mg/kg/day of apocynin dissolved in 50% DMSO ($n = 5$ each). All reagents were purchased from Sigma-Aldrich (St Louis, MO). To implant the osmotic micropumps, mice were anesthetized with 1.5% isoflurane (Isoflurane florane, Baxter), and placed in prone position (see Halabi et al.⁶ for implantation procedure). As each osmotic pump is designed to deliver the reagent for 28 days, on day 28, the first pump was removed and replaced by a new pump using the same surgical technique. Physiological studies were done on day 56, when mice were euthanized. At replacement and death, pumps were removed, and delivery of the drug was confirmed by assessing the volume of solution remaining in each pump.

Acute Apocynin Treatment

To determine the effect of acute apocynin treatment, 3-month-old male $\text{Eln}^{+/-}$ mice were treated with 3 doses of 12 mg/kg apocynin. Baseline BP was measured by placing a Millar pressure-transducing catheter (Millar Instruments, Houston, TX) in the right carotid artery under 1.5% isoflurane, as previously described.²⁴ The left jugular vein was then isolated and cannulated with PE-10 tubing (Instech, Plymouth Meeting, PA) preloaded with either 3 20 μL doses of vehicle (20% DMSO) or 3 20 μL doses of 12 mg/kg drug, apocynin. Isoflurane was decreased to 1% and a baseline BP established. Bolus injections of either drug or vehicle were then administered allowing BP to recover between doses. Systolic BP (SBP) was measured preinjection and 30 s postinjection. SBP changes resulting from either apocynin or vehicle injection are represented as SBP percent reduction which was calculated by: $([\text{SBP at 30 s} - \text{baseline SBP before injection}]/\text{baseline SBP before injection}) \times 100$. SBP reduction was compared between the acute apocynin treatment group and vehicle/control.

SBP and Heart Rate Measurement

The narrow diameter and tortuous nature of $\text{Eln}^{+/-}$ carotid arteries limit the placement and continued function of indwelling radiotelemeters. Consequently, this study uses a smaller, acutely placed angiocatheter to measure BP. To achieve this

measurement, mice were restrained on a heated holder to maintain body temperature, anesthesia induced with 2.5% inhaled isoflurane, then reduced to 1.5% to achieve a level plane of anesthesia. A 1.4F pressure catheter ($\text{Ncf1}^{+/-}$ experiments), model SPR671 or 1.0F ($\text{Nox}^{-/\gamma}$ experiments), model SPR1000, Millar Instruments, Houston, TX) was introduced into the right carotid artery and advanced to the ascending aorta. Each animal was allowed to acclimate for 5 min, at which time isoflurane was reduced to 1%. Pressures were recorded using Chart 5 software (ADInstruments, Colorado Springs, CO) and analyzed from 1 to 4 min post reduction.⁵ Animals were monitored for discomfort or over-sedation.

Assessment of Aortic Stiffness (Pulse-Wave Velocity)

Aortic-arch pulse-wave velocity (PWV) was performed as previously described⁵ using a modification of the transit-time method on a Vevo 770 ultrasound system with a MS-400 transducer (VisualSonics Inc., Toronto, Canada). In some cases (typically the $\text{Eln}^{+/-}$ mice, due to their longer and more tortuous aortas), vessels could not be imaged in a single plane. For these animals, the pulse-wave Doppler was performed in 2 segments. First, a proximal measurement was taken near the aortic valve and then the probe was quickly moved to the adjacent descending aorta without changing the imaging plane. The curvilinear distance between the proximal and distal points of the aortic velocity interrogation (D2–D1) was measured, as well as the time delay between the onset of flow velocity in the distal and proximal portions of the aorta (T2–T1) relative to the simultaneously recorded electrocardiogram signal. $\text{PWV} = (\text{D2} - \text{D1}) / (\text{T2} - \text{T1})$.

Histological Analysis

Mice were flushed with PBS via the left ventricle and then, using a syringe pump (Model 200, Cole-Parmer, Vernon Hills, IL), the vasculature was fixed with 10% buffered formalin (Sigma) at a constant flow rate of 1.5 mL/min. The ascending aorta was excised, placed in 10% formalin overnight, transferred to 70% ethanol, embedded in paraffin, and then serially sectioned at 5 μm . For mesenteric samples, a segment of the first-order mesenteric artery branch was freed of fat and connective tissue under a dissection microscope before being processed. Verhoeff-van Gieson (VVG) stain was used to assess ELN, whereas Masson's trichrome stain was used to assess collagen. Movat stain can simultaneously detect collagen and ELN. All stains were performed according to the product instructions. Stained slides were scanned using a Nanozoom RS digital slide scanner (Hamamatsu) and analyzed using NDP Viewer software (Hamamatsu Photonics, Hamamatsu, Japan). Wall thickness, lumen area, and lamellar number were determined using methods previously described.⁵

Pressure–Diameter Testing

Ascending aortas were dissected from mice post euthanasia. Vessels were mounted on a pressure arteriograph (Danish Myotechnology, Copenhagen, Denmark) in PSS at 37°C. Vessels were then pressurized and longitudinally stretched 3 times to in vivo length^{5,16} before data capture. Arteries were transilluminated under a microscope connected to a camera and computerized measurement system (Myoview, Danish Myotechnology). Intravascular pressure was increased from 0 to 175 mmHg in 25 mmHg steps. At each step, the outer diameter of the vessel was measured and manually recorded. Functional distensibility (FD) was calculated from the pressure diameter curves as the

distensibility at average working pressure of the vessel: $FD = (OD_{SBP} - OD_{DPB}) / (OD_{DPB}) / (SBP - DPB)$, where $OD =$ outer diameter at either SBP or DPB. For pressures that fall between diameter measurement intervals, the working diameter at the specific pressure was calculated using the known slope of the line between the preceding and subsequent pressure for that animal.

Measurement of Oxidative Modification of DNA: 8-Hydroxyguanosine Immunohistochemistry

Ascending aorta and first-order branch mesenteric arteries were dissected and fixed in 10% buffered formalin overnight, before transfer to 70% ethanol. Fixed samples were then embedded in paraffin and 10- μ m-thick sections were cut and placed on glass slides. Before immunofluorescence analysis, sections were deparaffinized, rehydrated, and boiled in 10 mM citrate buffer (pH 6.0) for 10 min for antigen retrieval. Sections were then blocked for 1 h in 10% normal donkey serum in PBS, and subsequently incubated with goat polyclonal antibody against 8-hydroxyguanosine (8OH, a DNA oxidative marker) (50 μ L, 1:200, Abcam, San Francisco, ab10802) in 2% donkey serum in PBS overnight in a humidified chamber at 4°C. After 3 washes in PBS, sections were incubated with Alexa-fluor-594 donkey anti-goat antibody (2 mg/mL, 1:500, Abcam, San Francisco, ab150132) for 60 min at room temperature in the dark. Sections were then rinsed in PBS and sealed with mounting medium containing DAPI (Vectashield, Burlingame, H-1200). Images were captured from each section using a Zeiss 780 inverted confocal microscope at $\times 40$ magnification (Ex:Em = 594 nm/588–695 nm). To quantify immunofluorescence, each aortic sample was imaged in 4 quadrants and quantifications were done in each quadrant and averaged together. Mesenteric artery samples were imaged and quantified using a single image. Staining intensity was measured in the endothelium and media for aortic and mesenteric artery samples. This region was defined by manually outlining the area within and the external elastic lamina and using the lumen as the internal boundary. Average corrected fluorescence intensity of the 8OH was measured in defined regions of interest using ImageJ software (National Institutes of Health, Bethesda, MD) and data are expressed as fluorescence signal per area, as previously described.^{25,26} To account for variability, the imaging was done using identical conditions of magnification, illumination, and exposure time.

Response to Vasoactive Medications

To evaluate the impact of various vasoactive drugs on animal physiology, a central venous catheter (PE-10 tubing, Instech, Plymouth Meeting, PA) was placed in the jugular vein of $Eln^{+/+}$, $Eln^{+/-}$, and $Eln^{-/-}$; $Nox1^{-/-}$ mice sedated with isoflurane. An arterial pressure catheter (Millar Instruments, Houston, TX) was also placed as noted above to measure continuous pressure and heart rate. To assess physiological response to vasoconstriction, baseline BP was established, and mice were then injected with increasing bolus concentrations (10 μ g/kg, 100 μ g/kg, 1 mg/kg) of PE diluted in PBS. In subsequent experiments, $Eln^{+/-}$ and $Eln^{+/+}$ mice were injected with either tempol (Sigma, St Louis, 176141, 50 mg/kg), PE (100 μ g/kg), or consecutive doses of tempol/PE (50 mg/kg tempol and 100 μ g/kg of PE). Similarly, to assess physiological response to acetylcholine, baseline BP was established, and mice were then injected with increasing bolus concentrations (1, 10, and 100 μ g/kg) of ACh (Sigma, St Louis, MO) diluted in PBS. BP and heart rate were monitored throughout the procedure, and the animal's BP was allowed to return to baseline

before administration of the next dose. Response to vasoactive drugs was calculated as percent change in SBP: $([SBP - SBP_i] / SBP_i) \times 100$, where SBP_i is the initial SBP before injection of the drug(s), and SBP maximal deviation from baseline after drug administration(s) before return to baseline. Each drug combination (PE alone, tempol alone and tempol plus PE, or ACh alone in the ACh experiment) was given twice during the 50-min experiment and the mean value of the 2 doses was used for statistical assessment.

Statistics

All statistics were performed using Prism 7.0 statistical software. BPs, FD, histological quantification, and PWV were compared in $Eln^{+/+}$ and untreated and treated (drug or Nox mutant) 3-month-old $Eln^{+/-}$ mice using one-way analysis of variance (ANOVA). For pressure–diameter, distensibility and vasoactive drug testing, two-way ANOVA with repeated measures were used. When appropriate, multiple comparisons testing were performed, and test type is reported in the legend for each figure. Multiple t-tests were performed for the acute apocynin and tempol experiments with an False discovery rate (FDR) of 0.05 used for discovery phase.

Results

Increased Oxidative Stress in $Eln^{+/-}$ Relative to $Eln^{+/+}$ Mouse Aorta

Oxidative stress is known to be implicated in the pathophysiology of hypertension.²⁷ Recent studies have shown a correlation between ELN insufficiency and increased ROS production, suggesting that oxidative stress may play a role in hypertension in the $Eln^{+/-}$ mouse.^{8,9,28} To confirm the effect of ELN insufficiency on vascular ROS production, we stained sections of $Eln^{+/-}$ and $Eln^{+/+}$ aorta with the superoxide sensitive stain, DHE. In the presence of superoxide, DHE is oxidized to a fluorescent adduct that intercalates into DNA, producing a nuclear staining pattern. The degree of staining correlates with superoxide production by the tissue. In agreement with previously published studies,^{9,28,29} DHE fluorescence was visibly higher in the endothelium/media of the $Eln^{+/-}$ aorta relative to the $Eln^{+/+}$ (Figure 1A and B).

$Eln^{+/-}$ Vascular Anomalies Result in Turbulent Flow: Loss of Flow Reduces ROS

It has previously been suggested that hemodynamic forces, such as shear stress resulting from turbulent blood flow, can either directly or indirectly activate vascular NADPH oxidase-derived ROS production.^{30–33} Previous reports of the $Eln^{+/-}$ mouse have noted a decrease in vascular caliber and an increase in wall thickness with increased small and large vessel tortuosity.^{14–16} To assess for changes in flow parameters in this animal model, we made use of high-resolution, high-frame rate 2D echocardiogram to visualize flow in the aortic arch. The images show fine anatomical details of the $Eln^{+/+}$ arch (Figure 2A) and demonstrate marked tortuosity of the $Eln^{+/-}$ aorta (Figure 2B), with elongation of the ascending aorta and abnormal orientation of its proximal branches. Video S1 ($Eln^{+/+}$) shows normal biphasic pulsatile laminar flow with predominant systolic but also lower velocity diastolic antegrade flow. Alternatively, Video S2 ($Eln^{+/-}$) shows rapid cessation of antegrade flow in end-systole with short duration retrograde flow in early diastole and static flow during midlate diastole,

implying turbulence and oscillatory flow. Doppler interrogation of the aortic valve showed no aortic regurgitation. Oscillatory (disturbed) flow has been linked to increased ROS production.^{32,34,35}

To determine whether hemodynamic differences present in *Eln*^{+/-} mice are responsible for increased ROS production, we cultured sections of ascending aortas from these mice for 16 h under flow-free conditions before evaluating for ROS. When cultured in the absence of flow for 16 h, both *Eln*^{+/+} and *Eln*^{+/-} aortas revealed low-level superoxide production and there was no obvious difference between the 2 (Figure 1C and D). The average

DHE intensity per pixel in each endothelial and medial nucleus was determined (Figure 1E). Two-way ANOVA found a significant *Eln* effect ($P < 0.05$), a significant treatment effect ($P < 0.01$), and a borderline interactive effect ($P = 0.05$). DHE fluorescence intensity was found to be significantly greater in the real time *Eln*^{+/-} group relative to all other subgroups ($P < 0.05$ or better). Antimycin A added after the 16-h culture period to a second section of aortic tissue confirmed that the cells from the cultured vessels were capable of producing ROS at similar levels (Figure S2A–C). Likewise, real time and flow-free vessels were evaluated for response to PE on a ring myograph. All vessels

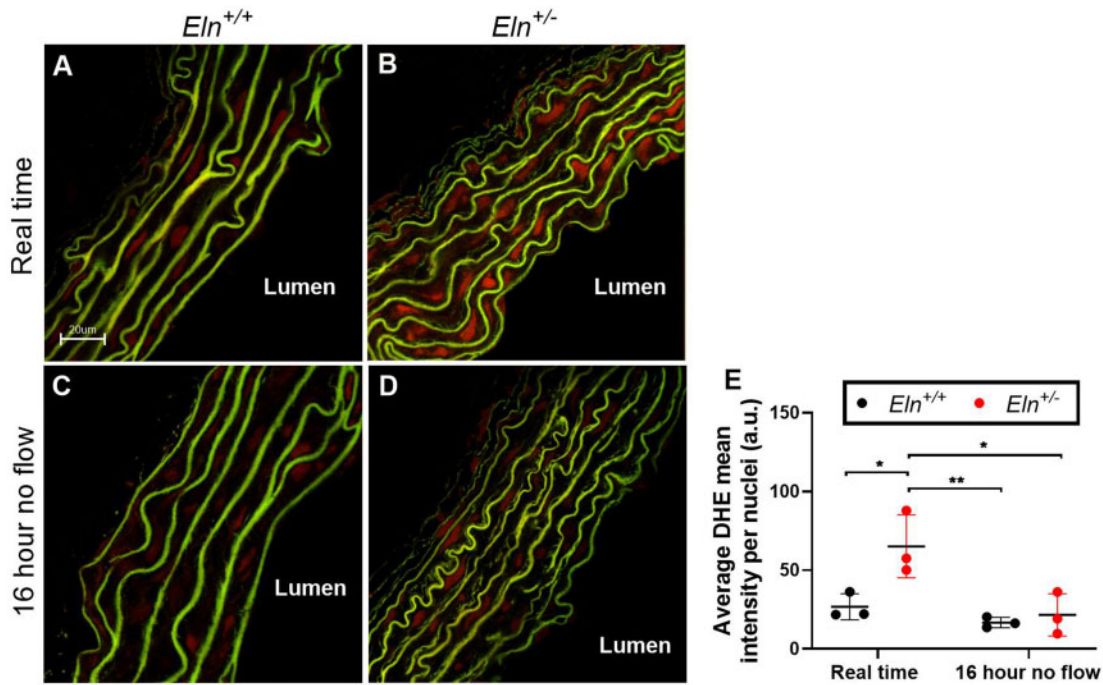


Figure 1. Hemodynamic Forces Influence ROS Production in *Eln*^{+/-}. (A [*Eln*^{+/+}] and B [*Eln*^{+/-}]) Confocal images of aortic tissue stained with DHE immediately after dissection. (C [*Eln*^{+/+}] and D [*Eln*^{+/-}]) Confocal images of aortic tissue sections stained with DHE after a 16-h incubation in culture media. Average DHE mean fluorescence intensity per nuclei (E). Tukey's multiple comparisons test: * $P < 0.05$ and ** $P < 0.01$ between indicated groups.

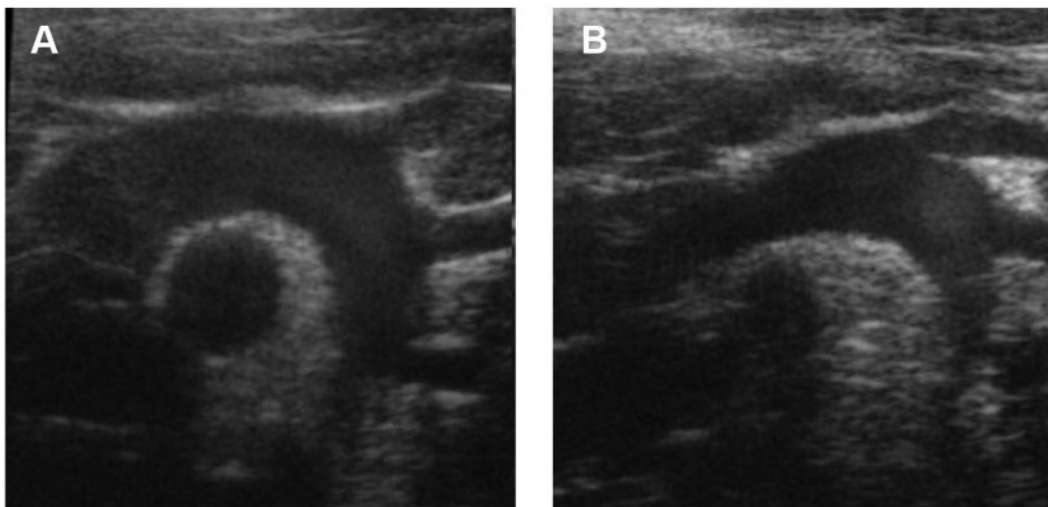


Figure 2. High-resolution, High-frame Rate 2D Echocardiogram of the *Eln*^{+/+} and *Eln*^{+/-} Aortic Arch. Still images from the ECG-gated KiloHertz Visualization image acquisition show a normal appearing aortic arch in the *Eln*^{+/+} (A) and marked tortuosity of the *Eln*^{+/-} (B) aorta, with elongation of the ascending portion and abnormal orientation of the proximal branches. The bright regions in the arch lumen represent jets of blood. Videos S1 (*Eln*^{+/+}) and S2 (*Eln*^{+/-}) show the movement of blood through the arch, highlighting the turbulence apparent in the *Eln*^{+/-}.

showed the expected PE dose effect (Figure S2D; $P < 0.01$) and there was no contraction difference between the real time and flow-free vessels.

Chronic, but not Acute, Apocynin Treatment Lowers SBP in $Eln^{+/-}$ Mice

To determine the source of ROS in $Eln^{+/-}$ vessels, we treated mice with apocynin, an NADPH oxidase inhibitor. Apocynin blocks the phosphorylation of p47phox, the regulatory subunit of the NOX1 and 2 and thus prevents their activation.² Chronically inhibiting NOX activation through long-term administration of apocynin (3 mg/kg/day from weaning to 3 months of life) leads to lower SBP in $Eln^{+/-}$. Two-way ANOVA analysis of the chronic apocynin-treated groups showed an *Eln* effect ($P < 0.001$) and an interactive effect ($P < 0.05$), with a significantly lower SBP in the $Eln^{+/-}$ treated with apocynin than in carrier-treated $Eln^{+/-}$ ($P < 0.05$), whereas the $Eln^{+/+}$ was unaffected by chronic apocynin treatment (Figure 3A). Because of the mechanism of action, acute treatment with apocynin would be expected to block the production of new ROS by NOX but would not scavenge/reduce existing ROS. Unlike the chronic treatments, 3 consecutive 20 μ L doses of 12 mg/kg of apocynin over 30 min, in 3-month-old mice yielded no change in SBP in $Eln^{+/-}$ by unpaired t-test (Figure 3B).

Decreased *Ncf1* expression reduces BP and improves vascular stiffness in $Eln^{+/-}$ mice

Previous studies in humans and mice with the WS deletion showed that larger deletions that included the nearby *NCF1* gene (individuals were left with 1 rather than 2 functional copies of the gene) were associated with lower BP.^{7,8,28} *NCF1* is the gene that encodes for p47phox, the molecule inhibited by apocynin. Focusing on the specific interaction between *Eln* and *Ncf1* haploinsufficiency, we measured BP and vascular stiffness in ~3-month-old progeny from an $Eln^{+/-} \times Ncf1^{+/-}$ cross. Invasive BP monitoring (Figure 4A) showed an expected *ELN* effect on SBP ($P < 0.0001$, 2-way ANOVA), an *Ncf1* effect ($P < 0.05$), and an interactive effect ($P < 0.05$). As expected, a significant difference between $Eln^{+/-}$ and $Eln^{+/+}$ mice, regardless of *Ncf1* genotype, was noted ($P < 0.0001$). Just as inhibition of p47phox by apocynin reduced SBP in the $Eln^{+/-}$ mice, *Ncf1* heterozygosity also led to a significant decrease in SBP in $Eln^{+/-}$ s ($P < 0.05$), while it had no effect on $Eln^{+/+}$ BP. In addition to BP differences, previous studies also showed that patients with the WS deletion that

included *NCF1* also had reduced PWV, an in vivo measure of vascular stiffness. Similarly, PWV evaluation in mice revealed a significant *Eln* effect ($P < 0.0001$, 2-way ANOVA) with $Eln^{+/-}$ mice having higher PWV and stiffer aortas (Figure 4B). The 2-way ANOVA also showed an *Ncf1* effect ($P < 0.05$) as well as an interactive one ($P < 0.01$). A robust reduction in PWV was found in $Eln^{+/-}; Ncf1^{+/-}$ mice as compared with those $Eln^{+/-}; Ncf1^{+/+}$ ($P < 0.01$), whereas *Ncf1* dosage had no significant impact on PWV in $Eln^{+/+}$ mice.

Biomechanical Properties and ELN Composition of $Eln^{+/-}$ Aortas are not Modified by *Ncf1* Expression

Aortic tissue was assessed using VVG (ELN) and Masson's Trichrome (collagen) stains to determine the impact of *Ncf1* dosage on vessel structure (Figure 5A–H). No obvious differences in collagen composition (blue) were noted between $Eln^{+/+}$ and $Eln^{+/-}$ samples, regardless of *Ncf1* mutant status (Figure 5E–H). Lamellar number is higher in $Eln^{+/-}$ ascending aorta ($P < 0.0001$, 2-way ANOVA), this difference is not impacted by *Ncf1* genotype (Figure 5I). Neither *Eln* nor *Ncf1* genotype had an effect on medial area (Figure 5J). To investigate how *Ncf1* insufficiency impacts stiffness, we evaluated the biomechanical properties of the aorta by generating pressure–diameter curves (Figure 5K). Although the test showed the expected difference between $Eln^{+/+}$ and $Eln^{+/-}$ mice (2-way ANOVA, genotype effect $P < 0.0001$), with $Eln^{+/-}$ mice being narrower and stiffer, the addition of *Ncf1* insufficiency did not influence the pressure–diameter relationship in either ELN genotype.

Improved distensibility in $Eln^{+/-}; Ncf1^{+/-}$ aorta

Medications and conditions that lower SBP have the potential to alter functional stiffness by shifting the working pressure of a vessel to a more compliant portion of the pressure–diameter curve.^{6,27,36} Consequently, we hypothesized that lower SBP in the $Eln^{+/-}; Ncf1^{+/-}$ may have the same effect. To test this, we calculated FD for each animal using working BP (Figure 5L). FD is a measure of the change in diameter a vessel sees when measured at its systolic and diastolic BP, normalized to the change in pressure (see “Materials and Methods” for full description). A 2-way ANOVA found in FD is significantly lower in the $Eln^{+/-}$ mouse relative to $Eln^{+/+}$ (*Eln* effect < 0.0001 , *Ncf1* effect $P < 0.001$, and interactive effect < 0.0001), with a significant difference between the $Eln^{+/-}$ groups depending on *Ncf1* genotype ($P < 0.0001$). However, $Eln^{+/-}; Ncf1^{+/-}$ mice have an FD that is more similar to

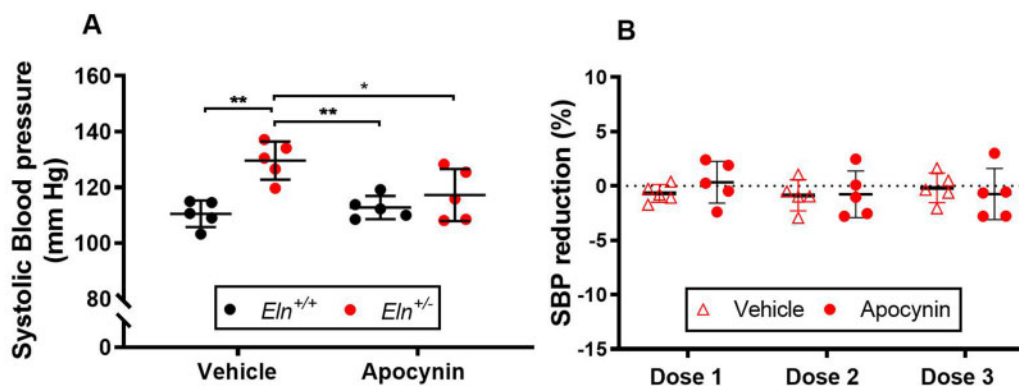


Figure 3. Chronic Reduction of ROS in *Eln* Insufficiency Reduces BP, Whereas Acute Reduction has no Impact. (A) SBP from $Eln^{+/+}$ and $Eln^{+/-}$ mice, after chronic infusion 50% DMSO carrier alone or apocynin in 50% DMSO. Tukey's multiple comparisons test: * $P < 0.05$ and ** $P < 0.01$. (B) Percent SBP change in $Eln^{+/-}$ after acute treatment with 3 doses of apocynin. No significant differences were noted by multiple t-test.

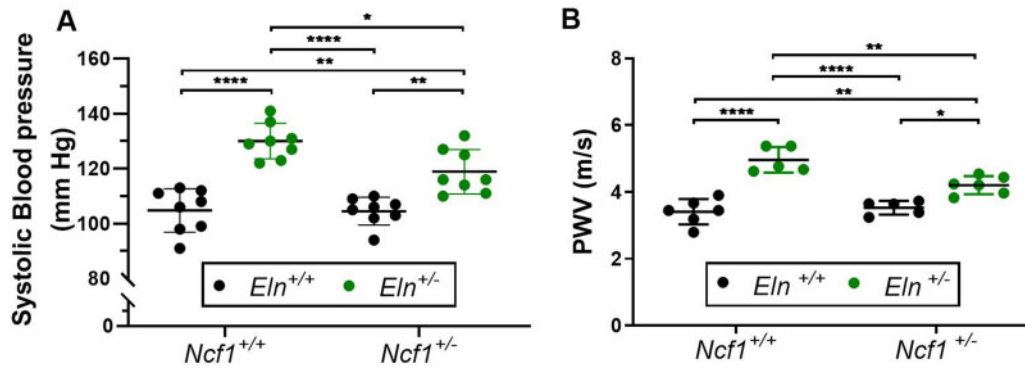


Figure 4. Reduced *Ncf1* Expression is Associated with Lowered BP and PWV in *Eln*^{+/-}. (A) SBP and (B) PWV from *Eln*^{+/-} × *Ncf1*^{+/-} cross. Tukey's multiple comparisons test: **P* < 0.05, ***P* < 0.01, and *****P* < 0.0001.

Eln^{+/-}; *Ncf1*^{+/-} mice. Because *Eln*^{+/-}; *Ncf1*^{+/-} mice experience no SBP reduction with the addition of *Ncf1* heterozygosity, the *Eln*^{+/-}; *Ncf1*^{+/-} FD remains similar to the *Eln*^{+/-}; *Ncf1*^{+/+}.

NOX1 plays the Dominant Role in Modulating Vascular Phenotypes of *Eln*^{+/-} Mice

Ncf1(p47phox) is a regulatory subunit of NOX1 and NOX2 NADPH oxidase complexes. The NOX1 complex is detectable in endothelial and SMCs and NOX2 in endothelial and inflammatory cells associated with the adventitia. Both genes are present on the X chromosome in mice and humans and both have been implicated in BP differences in angiotensin infusion models. However, none of them has been evaluated in genetic/developmental models of hypertension, such as the *Eln*^{+/-} mouse. Evaluation of the *Eln*^{+/-}; *Nox2*^{-/-} mutant showed an insignificant effect on SBP (2-way ANOVA, *Eln* effect *P* < 0.001, *Nox2* effect and interactive effects *P* = NS) (Figure 6A). Invasive BP monitoring in the *Eln*^{+/-}; *Nox1*^{-/-}, on the other hand, revealed both the expected ELN associated with increased SBP and a strong *Nox1* effect on SBP (2-way ANOVA, *P* < 0.01 for ELN effect, *P* = 0.01 for *Nox1* effect) that was more pronounced in the *Eln*^{+/-}; *Nox1*^{-/-} (interactive effect [*P* < 0.01, multiple comparisons results shown in Figure 6C]). Unlike the *Eln*^{+/-}; *Ncf1*^{+/-} mutant which displays a moderate drop in SBP relative to the *Eln*^{+/-}; *Ncf1*^{+/+}, the *Eln*^{+/-}; *Nox1*^{-/-}'s SBP is reduced to an *Eln*^{+/+} level. And again, neither *Nox1* nor *Nox2* deficiency had an effect on the pressure-diameter relationship of mutant aortas (Figure 6B and D), and there was no change in the histological appearance of the *Nox*^{-/-} vessels relative to their matched *Eln* genotype control (*Nox1*^{-/-} shown in Figure S3A-F) and no change in *Eln*^{+/-} lamellar number (Figure S3G).

NADPH Oxidase Mutants Display Reduced Detectable ROS

Given the more robust phenotypic change seen in the *Eln*^{+/-}; *Ncf1*^{+/-} and the *Eln*^{+/-}; *Nox1*^{-/-}, we further assessed ROS in the *Eln*^{+/-} and *Eln*^{+/+} aortas, with and without *Ncf1* or *Nox1* mutation by measuring 8OH by immunofluorescence. The anti-8OH antibody binds DNA that has been modified by ROS, giving a relative measurement of chronic ROS exposure for a tissue. Similar to the DHE experiment in Figure 1, 8OH was found to be significantly greater in the *Eln*^{+/-} relative to the *Eln*^{+/+} (Figure 7A, B and D, E, quantification in Figure 7G and H). In both the *Ncf1* and the *Nox1* experiments, a significant difference in 8OH fluorescence was found between the groups by 1-way

ANOVA (*P* < 0.01 in the *Ncf1* experiment and *P* < 0.0001 in the *Nox* experiment). In each case, a difference between the *Eln*^{+/-} and *Eln*^{+/+} was found (*P* < 0.01 or better; Figure 7G and H). And in both cases, reduction of *Nox* subunit dosage reduced 8OH-guanosine detected (Figure 7C and F). As expected by the gene dosage (heterozygous versus complete knockout) and the SBP findings, the normalization of ROS was more apparent in the *Nox1*^{-/-} mutants (*P* < 0.0001) than in the *Ncf1*^{+/-} (borderline effect *P* = 0.06).

NOX Expression Effect on Mesenteric Arteries

Because BP is controlled in the resistance vasculature rather than the large arteries, we examined the properties of the mesenteric artery. Consistent with previous observations,²⁴ the internal and external lamellae of the *Eln*^{+/-} mesenteric artery are thinner and less defined compared with the *Eln*^{+/+} (Figure 8A and B). However, we did not find the previously reported difference in lamellar number between the 2 ELN genotypes,²⁴ with both having internal, external, and middle (sometimes discontinuous) lamellae. The *Eln*^{+/-}; *Nox1*^{-/-} double mutants are structurally similar to the *Eln*^{+/-}; *Nox1*^{+/+} vessels (Figure 8C). However, 8OH-guanosine staining revealed a similar pattern as in the large vessels; an increase in the *Eln*^{+/-} that is lost in the *Nox* mutants (quantification only shown in Figure 8D).

PE Response is Modulated by ROS

Oxidative stress is known to play a role in controlling vasoreactivity.^{3,37} To identify differences in vascular responsiveness in our mouse models, we assessed SBP changes following in vivo bolus injections of PE (Figure 9A) and ACh (Figure S4). A 2-way ANOVA of the PE experimental data showed a significant PE dose effect (*P* < 0.0001), a genotype effect (*P* < 0.01), and a significant interactive effect (*P* < 0.001). Both *Eln*^{+/+} and *Eln*^{+/-} mice have a similar response to low-dose PE (10 μg/kg). Multiple comparisons analysis found the response to 100 μg/kg of PE was significantly augmented in the *Eln*^{+/-} mouse which showed a significant pressure spike (*P* < 0.0001) relative to the *Eln*^{+/+}. The *Eln*^{+/-}; *Nox1*^{-/-} double mutant, however, lacked the augmented response to the 100 μg/kg dose of PE. The differential response for the *Eln*^{+/-} mouse was maintained at the highest PE dose (1 mg/kg) as well (*P* < 0.05 versus *Eln*^{+/-}; *Nox1*^{-/-} and *P* < 0.01 versus *Eln*^{+/+}). A 2-way ANOVA of the ACh evaluation showed a significant ACh dose effect (*P* < 0.0001) with no significant genotype or interactive effect.

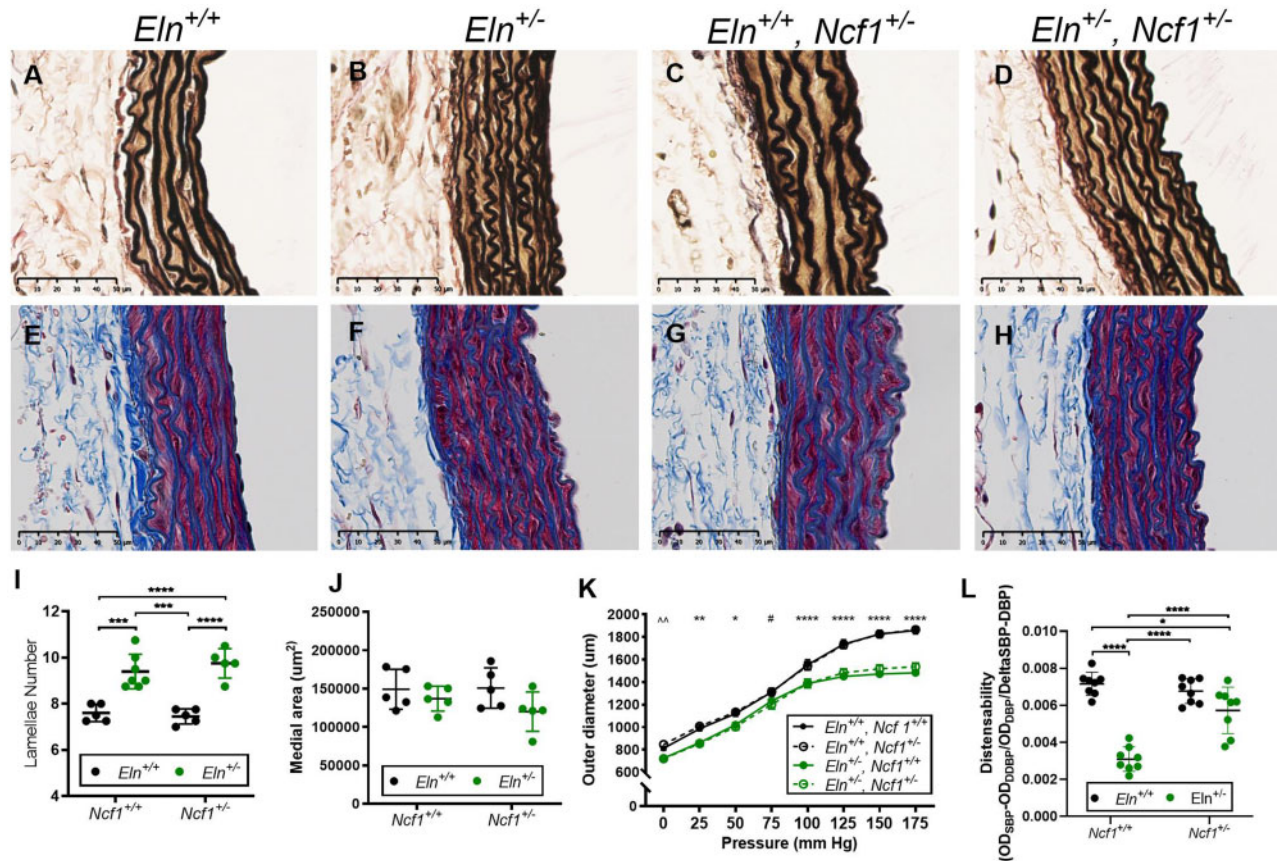


Figure 5. *Ncf1* Haploinsufficiency Reduces Blood Pressure without Biochemical or Structural Changes to the *Eln*^{-/-} Vasculature. Representative histological staining of ascending aorta in VVG (A–D) and Tri-chrome Masson (E–H), $\times 40$ in progeny from *Eln*^{+/-} \times *Ncf1*^{+/-} cross. (I) Elastic lamellar number was higher in *Eln*^{+/-}, regardless of *Ncf1* genotype and (J) medial area were similar among groups. (K) Aortic pressure–diameter curves show an *Eln* genotype difference but no within *Eln*^{+/-} genotype *Ncf1*^{+/-} effect. (L) Distensibility was measured as slope of pressure/diameter curve at the animals physiologic BP. Distensibility is reduced in the *Eln*^{+/-}; *Ncf1*^{+/-} but is higher in the *Eln*^{+/-}; *Ncf1*^{+/-}. Tukey’s multiple comparisons test: For I and L, **P* < 0.05, ****P* < 0.001, and *****P* < 0.0001. For K, **P* < 0.05, ***P* < 0.01, and *****P* < 0.0001 for comparisons of *Eln*^{+/+} versus *Eln*^{+/-} regardless of *Ncf1* genotype, ^^*P* < 0.01 for comparison between *Eln*^{+/+}; *Ncf1*^{+/-} versus *Eln*^{+/-}; *Ncf1*^{+/+} and *Eln*^{+/+}; *Ncf1*^{+/-} versus *Eln*^{+/-}; *Ncf1*^{+/-} and #*P* < 0.05 for comparisons between *Eln*^{+/+}; *Ncf1*^{+/+} versus *Eln*^{+/-}; *Ncf1*^{+/-} and *Eln*^{+/+}; *Ncf1*^{+/-} versus *Eln*^{+/-}; *Ncf1*^{+/-}.

To determine if ROS play a role in causing the significant response difference at 100 μ g/kg PE, we used a known ROS scavenger, tempol (4-hydroxy-2,2,6,6-tetramethylpiperidine-1-oxyl) in *Eln*^{+/+} and *Eln*^{+/-}. Tempol was injected alone 30 s prior to the 100 μ g/kg PE injection (Figure 9B). SBP change from baseline after 50 mg/kg of Tempol was significantly larger in the *Eln*^{+/-} relative to the *Eln*^{+/+} (*P* < 0.01). As shown previously, the *Eln*^{+/-} had an augmented response to the 100 μ g/kg PE dose (*P* < 0.0001) when no tempol was administered; however, injecting tempol prior to PE removed the difference in percent SBP change between the *Eln*^{+/-} and *Eln*^{+/+}. The response to PE in the presence of tempol was found to be similar in the *Eln*^{+/-} and *Eln*^{+/+}.

Discussion

ELN insufficiency produces blood vessels with reduced lumen size, tortuosity, and altered vascular mechanics. People with WS have a contiguous deletion on chromosome 7 that removes the *ELN* gene in combination with approximately 24 other coding genes. In some cases, the deletion extends to include the *NCF1* gene on the telomeric end of the typical deletion. Patients with deletions that cover this gene, and hence retain only 1 functional copy of *NCF1*, have lower BP and PWV, a measure of vascular stiffness, than those with 2 copies.^{7,9,28} Subsequent

studies in WS deletion mouse models have confirmed that *Ncf1* haploinsufficiency reduces BP in the setting of the contiguous deletion.^{8,28} Likewise, a quantitative trait locus modifier study performed in C57Bl/6 *Eln*^{+/-} \times 129 \times 1/SvJ F2 mice identified *Ncf1* as a potential modifier for BP and aortic diameter.⁹ Each of these studies highlighted a role for NADPH oxidase-produced ROS in mediating BP and stiffness differences in this developmental disorder and recently investigators have implicated ROS produced by the NOS system in this phenomenon as well.³⁸

Much of the work in ROS-mediated hypertension published to date has focused on the ROS produced by inflammatory cells in the adventitia and perivascular fat in response to acute angiotensin infusion.^{39–41} The genetic model here is distinct from the acute induction of hypertension used in those experiments. In ELN insufficiency, the vascular defect is chronic as blood vessels exhibit obvious structural differences early in the postnatal period, with higher BPs noted by as early as postnatal day 1.⁴² Consequently, in ELN insufficiency, there is no abrupt physiological change prompting acute immune response at the age we are studying, rather the BP differences are chronic and likely mediated by other mechanisms.

In this study, we further drill down on the hypertension phenotype in this genetic model by reducing the potential genetic interaction from the larger WS deletion to a specific interaction between *Eln* and *Ncf1*. Although a more directly quantitative

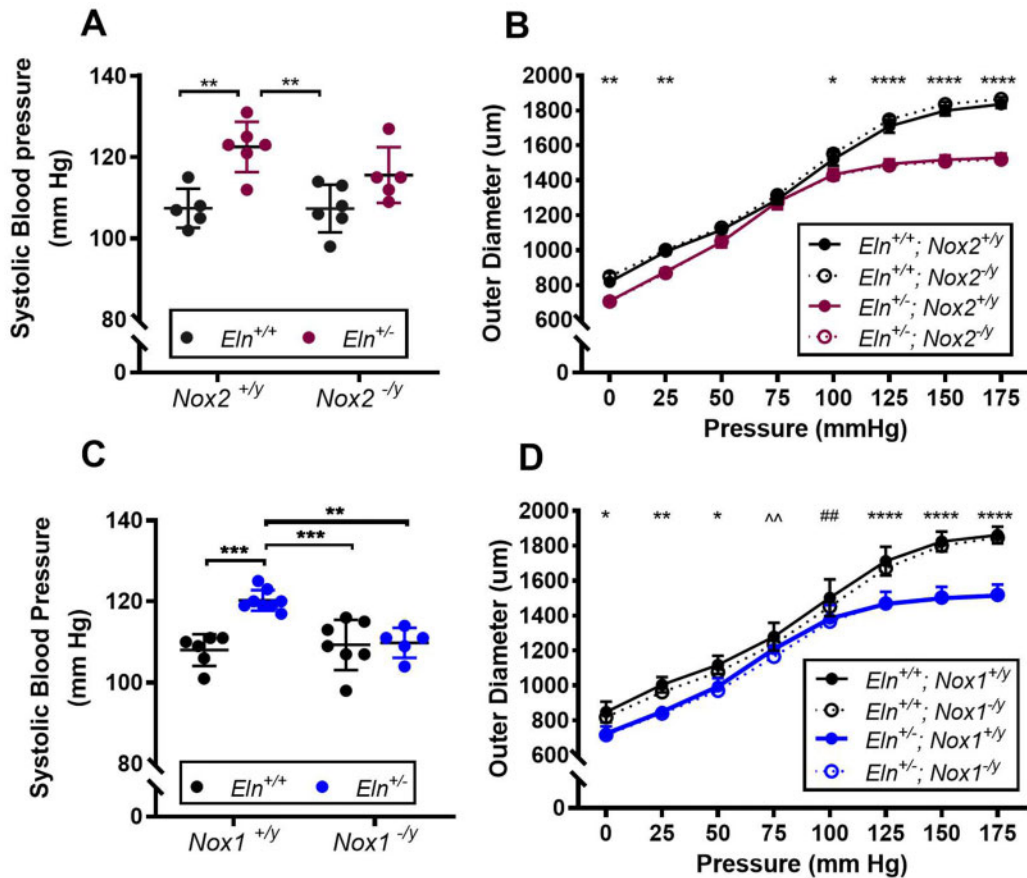


Figure 6. *Nox1* Deficiency Reduces SBP and Oxidative Stress in *Eln*^{-/-}. SBP data for (A) *Eln*^{-/-} × *Nox2*^{-/y} and (C) *Eln*^{-/-} × *Nox1*^{-/y} progeny. Tukey's multiple comparisons test: ***P* < 0.01 and ****P* < 0.001, *****P* < 0.0001 between indicated groups. *Nox2* (B) and *Nox1* (D) do not alter the pressure-diameter relationship in *Eln*^{+/+} or *Eln*^{-/-} aortas. Tukey's multiple comparison (B) **P* < 0.05, ***P* < 0.01, and *****P* < 0.0001 for comparisons of *Eln*^{+/+} versus *Eln*^{-/-} comparisons regardless of *Ncf* genotype. (D) **P* < 0.05, ***P* < 0.01, and *****P* < 0.0001 for comparisons of *Eln*^{+/+} versus *Eln*^{-/-} comparisons regardless of *Ncf* genotype. ##*P* < 0.01 for comparison between *Eln*^{+/+}, *Nox1*^{+/y} versus *Eln*^{-/-}, *Nox1*^{+/y} and *Eln*^{+/+}, *Nox1*^{+/y} versus *Eln*^{-/-}, *Nox1*^{-/y}. ^^*P* < 0.01 for comparison between *Eln*^{+/+}, *Nox1*^{+/y} versus *Eln*^{-/-}, *Nox1*^{-/y}.

method may have been improved our ability to measure tissue ROS,^{43,44} our 2 semi-quantitative methods confirmed evidence of increased ROS in ELN insufficient tissues, similar to previously published findings.^{9,28,29} In addition, our studies also show that ROS are not generated in excess the *Eln*^{-/-} aorta in the absence of flow. Oscillatory shear stress is a known inducer of ROS production^{32,34} and the anatomical differences associated with ELN insufficiency (narrow, stiff arteries with abnormal branching patterns^{1,5,15,29} and tortuosity) predispose vessels to increased shear as evidenced by the turbulent aortic arch flow detected in our high-resolution, high-frame rate 2D echocardiogram studies. Consequently, it is the abnormal vascular anatomy itself that predisposes to increased ROS and thus leads to hypertension.

Although additional computational or in vivo modeling (partial carotid ligation) could be done to further evaluate the impact of shear, the role of increase ROS in ELN insufficiency mediated vasculopathy is validated by the finding that decreasing *Ncf1* function by genetic (*Ncf1*^{-/-}) or chemical (chronic apocynin) means fails to reduce the BP in *Eln*^{+/+} animals—*Eln*^{+/+} vessels have normal levels of shear and produce minimal ROS at baseline. Consequently, limiting ROS-producing capacity by reducing *Ncf1* dosage has minimal impact in situations when ROS are not required. In the *Eln*^{-/-} case, however, turbulence is higher, leading to robust NOX-mediated ROS production. As a result, in this

setting, reduction of the p47phox regulatory subunit greatly impacts the amount of ROS that can be produced (Figure 10).

Ncf1/p47phox regulates the activity of 2 Nox complexes, *Nox1* and *Nox2*. *Nox1* is present in endothelial and SMCs, whereas *Nox2* is made by endothelial, adventitial, and inflammatory cells. Being in the endothelial layer, both NOXs have the potential to influence the response to oscillatory shear forces. Our physiological analyses, however, show the loss of *NOX1* to have a more robust effect on BP. Although *Nox2*^{-/y} status non-significantly reduces *Eln*^{-/-} SBP by a few mmHg, *Eln*^{-/-}; *Nox1*^{-/y} mice have BP that is equivalent to that of *Eln*^{+/+}. Consequently, it is possible that the increased pathogenicity could be related to the higher number of cells impacted by its loss (endothelial and SMC) or because of differences in regulation or basal activity of the 2 complexes.⁴⁵⁻⁴⁸ The decreased impact of *Nox2* insufficiency may be related to the chronic nature of the condition. Most of the studies on this mutant have implicated T-cell activity in the pathogenesis.^{40,49} The inflammatory response may be more relevant to the acute hypertension models than chronic developmental/structural ones such as the *Eln*^{-/-} mouse.

Previous investigations of *Nox1* have suggested that it functions in long-term regulation of BP by altering the composition of the vascular extracellular matrix.^{10,13,50} In our assessment, although ROS differences could be detected in both large and small *Eln*^{-/-} vessels, no obvious differences in matrix

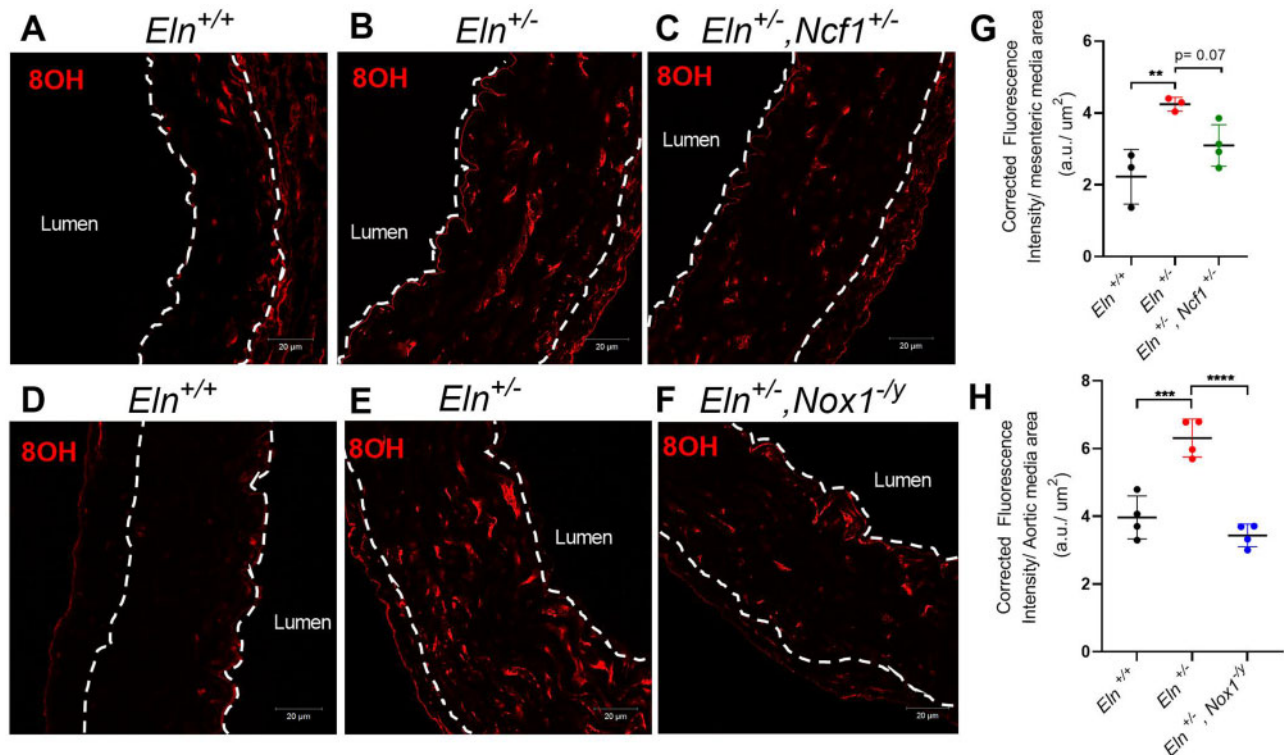


Figure 7. Increased Oxidative Stress in *Eln*^{+/-} is Modestly Reduced in the Presence of *Ncf1* Insufficiency. Sections of ascending thoracic aorta from *Eln*^{+/-} × *Ncf1*^{-/-} progeny (A–C) and *Eln*^{+/-} × *Nox1*^{-/-} (D–F) progeny were evaluated for the oxidative stress marker 8OH (×40). Red fluorescent signal (8OH) was assessed in the media (outlined by white hash marks), as defined by the area in between the internal and external elastic lamellae. (G) Comparison of average fluorescence intensity/area of 8OH in the *Ncf1* (G) and *Nox1* (H) experiments are shown. Tukey’s multiple comparison test, **P < 0.01, ***P < 0.001, and ****P < 0.0001.

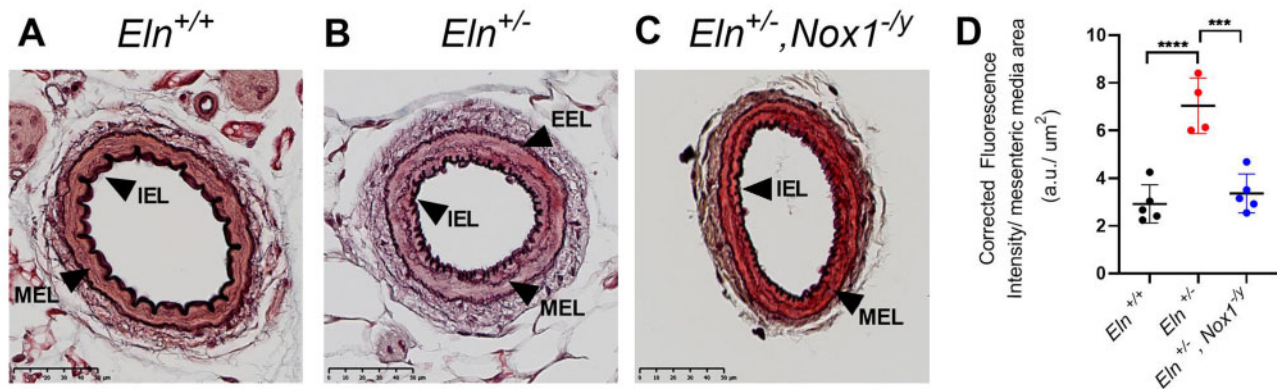


Figure 8. Increased ROS are Apparent in the *Eln*^{+/-} Mesenteric; Matrix Stain is Typical for *Eln* Genotype. (A–C) Representative Movat-stained histological sections of mesenteric artery showed no difference in ELN lamellar number between samples regardless of genotype. There is a visibly apparent difference in internal elastic lamellae (IEL) and external elastic lamellae (EEL) thickness. The *Eln*^{+/+} variant has a thicker IEL and EEL relative to the *Eln*^{+/-} and *Eln*^{+/-}, *Nox1*^{-/-}. *NOX* expression has no obvious impact on IEL or EEL thickness, with samples resembling *Eln*^{+/+}. A middle elastic lamella, MEL, was noted in all mesenteric samples, regardless of ELN or *NOX* expression differences. (D) Sections of primary branch mesenteric artery were sectioned and stained for oxidative stress using 8OH. 8OH fluorescence intensity measurements from the medial area. Tukey’s multiple comparison test, ****P < 0.0001 and ***P < 0.001.

composition were detected histologically. Likewise, pressure diameter curves were not altered in *Eln*^{+/-}; *Ncf1*^{+/-}, in *Eln*^{+/-}; *Nox1*^{-/-} or *Eln*^{+/-}; *Nox2*^{-/-} mutants. Consequently, previous differences noted in arterial stiffness in WS patients with reduced dosage of *NCF1*⁷ are likely secondary to the change in BP which alters the FD by moving the vessel to a more compliant portion of its pressure diameter curve.

Instead, we see that *Eln*^{+/-} mice have more dramatically increased BP in response to vasoconstrictors like PE. This general

finding has been described previously by Osei-Owusu et al.,²⁴ but our studies carry the finding further, showing that *Eln*^{+/-}; *Nox*^{-/-} mutants no longer have this amplified response. Likewise, tempol, a ROS scavenger, mitigates the response. Interestingly, treatment with apocynin, a drug that stops production of new ROS rather than scavenges them, has no effect when used acutely in this model. This finding may suggest that the impact of ROS is more chronic by modifying the production, stability, or activity of receptors to vasoconstrictors such as

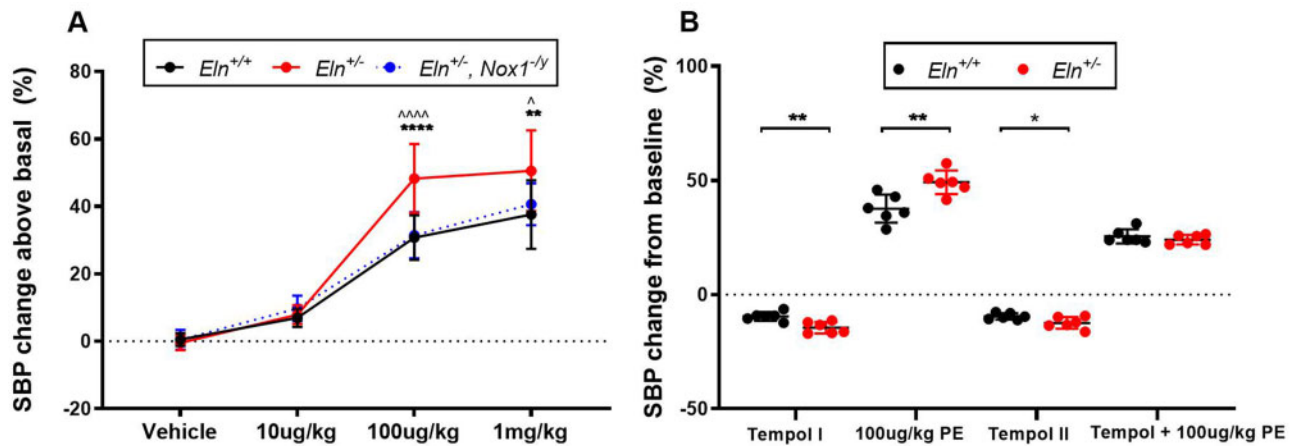


Figure 9. Augmented Phenylephrine Response in *Eln*^{+/-} is Mitigated by Nox Deficiency or Contemporaneous Tempol Treatment. (A) Percent SBP change after injection of increasing doses of PE. Tukey's multiple comparison test: ***P* < 0.01, *****P* < 0.0001 for comparison between *Eln*^{+/+} and *Eln*^{+/-}. ^*P* < 0.05, ^^^^*P* < 0.0001 for comparison between *Eln*^{+/+} and *Eln*^{+/-}, *Nox1*^{-/-}. (B) Percent SBP change after treatment with 50 mg/kg tempol, 100 μg/kg PE, or 50mg/kg tempol plus 100 μg/kg PE. Tukey's multiple t-test comparison test: **P* < 0.05 and ***P* < 0.01.

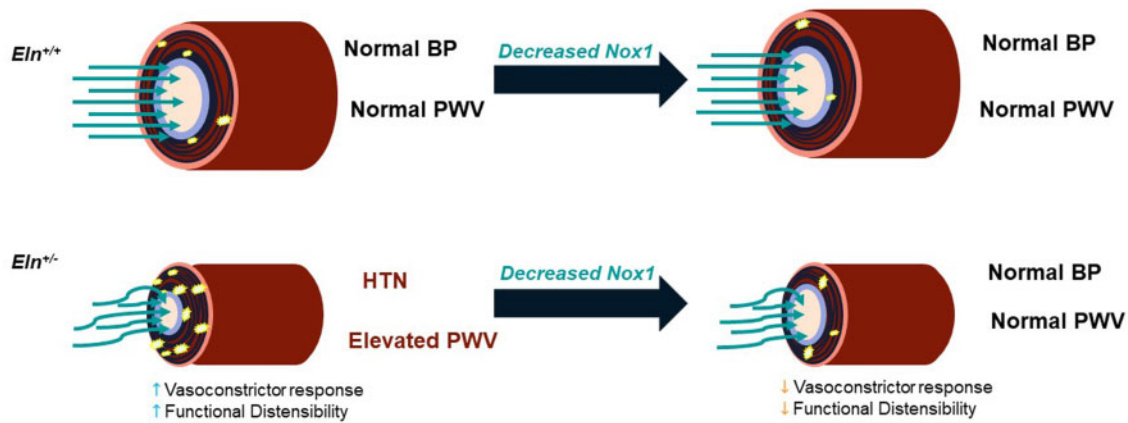


Figure 10. Loss of NOX1 Activity Reduces Blood Pressure and Functional Stiffness in *Eln*^{+/-} Mice. *Eln*^{+/+}; *Nox1*^{+/+} have normal caliber and experience laminar flow with relatively low shear. This combination results in low ROS production at baseline, yielding normal blood pressure and PWV. When Nox1 insufficiency is introduced in this background, the relative reduction of ROS is minimal and the change in blood pressure and PWV is negligible. In the *Eln*^{+/-}; *Nox1*^{+/+}, the narrow caliber and altered anatomy lead to oscillatory flow and increased shear, which produces a marked increase in ROS. In the high ROS *Eln*^{+/-} background, introduction of Nox1 insufficiency has the potential to dramatically reduce ROS, leading to altered vasoconstrictor response and lower blood pressure, which secondarily reduces FD and therefore PWV.

PE.²⁴ Indeed, several groups have shown the interaction between Nox activity and PE response,^{51,52} suggesting that both the endothelial and smooth muscle response to ROS are important in the pathophysiology of hypertension. Of particular note was the absence of a differential response of the *Eln*^{+/-} mouse to Ach. NOX-generated ROS are typically thought to limit endothelium-dependent relaxation.^{53,54} Normally, eNOS-produced NO diffuses across the endothelial layer and initiates a chain of events which ultimately decrease intracellular calcium levels, causing vasodilation.^{55,56} In the setting of increased NOX-generated ROS, however, superoxide anions generated by NOX react with NO to form peroxynitrite and reduce the availability of NO, therefore inhibiting relaxation. Previous studies have shown that overexpression of vascular smooth muscle NOX1 induces endothelial dysfunction and hypertension,⁵⁷ whereas reduction of Nox1 is associated with resistance to AngII-induced hypertension and decreased endothelial dysfunction.^{10,13} Consequently, one may have predicted the *Eln*^{+/-} mouse, with its increased ROS, to display evidence of endothelial

dysfunction and reduced dilation to Ach. Indeed, that is exactly what was shown after ex vivo interrogation of mesenteric and cerebral *Eln*^{+/-} arteries using myography techniques.^{24,29} Interestingly though, other arteries, such as the gastrocnemius, show no such differential response.²⁹ A similar vascular bed-specific response was seen in *Eln*^{+/-} vessels treated with AngII.⁵⁸ The in vivo technique shown here differs from the ex vivo ones used in the majority of the NOX and *Eln*^{+/-} published studies in that it reflects the response of the entire vascular tree (including vessels too small to sample on a myograph) to the vasoreactive stimulus and therefore may yield different results than the ex vivo measures.

Taken together, this study confirms that hypertension in *Eln*^{+/-} mice is mediated through NADPH-produced ROS and that reduction in those ROS through chemical or genetic means normalizes BP. Of the 2 Nox complexes with which p47phox (Ncf1) affiliates, inhibition of Nox1 has the more profound effect; its loss leading to complete normalization of the BP. This model differs from the Nox2-dominated effects seen in acute

hypertension models such as angiotensin infusion, potentially due the chronicity of the perturbation that likely minimizes any impact of inflammation.

Acknowledgments

The authors would like to thank Li Yi, Joshua Danback for their technical assistance and Mary Dinuer for the gift of Nox2^{-/-} mice. This manuscript used the light microscopy and the pathology core of the NHLBI DIR.

Authors' Contributions

A.T. and R.H.K. conducted experiments, acquired and analyzed data, and wrote the manuscript. C.M.H., A.W., E.K.K., D.M., Z.X.Y., K.M.T., A.K., and R.P.M. conducted experiments, acquired, and analyzed data. B.A.K. designed the study, analyzed data, and wrote the manuscript. All authors edited the manuscript.

Supplementary material

Supplementary material is available at the APS Function online.

Funding

Funding for this study was provided by the Division of Intramural Research at the National Heart, Lung, and Blood Institute of the National Institutes of Health (B.A.K. and NHLBI team members, ZIA HL-006212) and National Institutes of Health (R.P.M., R01-HL53325 and C.M.H. T32 HL007873 and K08 HL135400). Funding was also provided by the Ines Mandl Research Foundation (R.P.M.).

Conflict of Interest Statement

The authors state that they have no conflicts of interest to this study.

References

- Faury G, Pezet M, Knutsen RH, et al. Developmental adaptation of the mouse cardiovascular system to elastin haploinsufficiency. *J Clin Invest* 2003;112(9):1419–1428.
- Burtenshaw D, Hakimjavadi R, Redmond EM, Cahill PA. Nox, reactive oxygen species and regulation of vascular cell fate. *Antioxidants (Basel)* 2017;6(4):90.
- Touyz RM, Briones AM. Reactive oxygen species and vascular biology: implications in human hypertension. *Hypertens Res* 2011;34(1):5–14.
- Vaziri ND, Rodriguez-Iturbe B. Mechanisms of disease: oxidative stress and inflammation in the pathogenesis of hypertension. *Nat Clin Pract Nephrol* 2006;2(10):582–593.
- Knutsen RH, Beeman SC, Broekelmann TJ, et al. Minoxidil improves vascular compliance, restores cerebral blood flow, and alters extracellular matrix gene expression in a model of chronic vascular stiffness. *Am J Physiol Heart Circ Physiol* 2018;315(1):H118–H132.
- Halabi CM, Broekelmann TJ, Knutsen RH, Ye L, Mecham RP, Kozel BA. Chronic antihypertensive treatment improves pulse pressure but not large artery mechanics in a mouse model of congenital vascular stiffness. *Am J Physiol Heart Circ Physiol* 2015;309(5):H1008–1016.
- Kozel BA, Danback JR, Waxler JL, et al. Williams syndrome predisposes to vascular stiffness modified by antihypertensive use and copy number changes in NCF1. *Hypertension* 2014;63(1):74–79.
- Del Campo M, Antonell A, Magano LF, et al. Hemizygoty at the NCF1 gene in patients with Williams-Beuren syndrome decreases their risk of hypertension. *Am J Hum Genet* 2006;78(4):533–542.
- Kozel BA, Knutsen RH, Ye L, Ciliberto CH, Broekelmann TJ, Mecham RP. Genetic modifiers of cardiovascular phenotype caused by elastin haploinsufficiency act by extrinsic noncomplementation. *J Biol Chem* 2011;286(52):44926–44936.
- Matsuno K, Yamada H, Iwata K, et al. Nox1 is involved in angiotensin II-mediated hypertension: a study in Nox1-deficient mice. *Circulation* 2005;112(17):2677–2685.
- Drummond GR, Selemidis S, Griendling KK, Sobey CG. Combating oxidative stress in vascular disease: NADPH oxidases as therapeutic targets. *Nat Rev Drug Discov* 2011;10(6):453–471.
- Drummond GR, Sobey CG. Endothelial NADPH oxidases: which NOX to target in vascular disease? *Trends Endocrinol Metab* 2014;25(9):452–463.
- Gavazzi G, Banfi B, Deffert C, et al. Decreased blood pressure in NOX1-deficient mice. *FEBS Lett* 2006;580(2):497–504.
- Cocciolone AJ, Hawes JZ, Staiculescu MC, Johnson EO, Murshed M, Wagenseil JE. Elastin, arterial mechanics, and cardiovascular disease. *Am J Physiol Heart Circ Physiol* 2018;315(2):H189–H205.
- Li DY, Brooke B, Davis EC, et al. Elastin is an essential determinant of arterial morphogenesis. *Nature* 1998;393(6682):276–280.
- Wagenseil JE, Nerurkar NL, Knutsen RH, Okamoto RJ, Li DY, Mecham RP. Effects of elastin haploinsufficiency on the mechanical behavior of mouse arteries. *Am J Physiol Heart Circ Physiol* 2005;289(3):H1209–1217.
- Hawes JZ, Cocciolone AJ, Cui AH, et al. Elastin haploinsufficiency in mice has divergent effects on arterial remodeling with aging depending on sex. *Am J Physiol Heart Circ Physiol* 2020;319(6):H1398–H1408.
- Castellan RFP, Thomson A, Moran CM, Gray GA. Electrocardiogram-gated KiloHertz Visualisation (EKV) Ultrasound Allows Assessment of Neonatal Cardiac Structural and Functional Maturation and Longitudinal Evaluation of Regeneration After Injury. *Ultrasound Med Biol* 2020;46(1):167–179.
- Hilenski. Detection of ROS (O2 and H2O2) in vascular tissues In: Medicine E, ed. *Methods Used in Internal Medicine Imaging Core*. Atlanta, GA: Emory University School of Medicine, 2011:1–3.
- Williams IA, Allen DG. The role of reactive oxygen species in the hearts of dystrophin-deficient mdx mice. *Am J Physiol Heart Circ Physiol* 2007;293(3):H1969–H1977.
- Nijmeh J, Moldobaeva A, Wagner EM. Role of ROS in ischemia-induced lung angiogenesis. *Am J Physiol Lung Cell Mol Physiol* 2010;299(4):L535–L541.
- Gendron ME, Theoret JF, Mamarbachi AM, et al. Late chronic catechin antioxidant treatment is deleterious to the endothelial function in aging mice with established atherosclerosis. *Am J Physiol Heart Circ Physiol* 2010;298(6):H2062–2070.
- Drouin A, Farhat N, Bolduc V, et al. Up-regulation of thromboxane A(2) impairs cerebrovascular eNOS function in aging atherosclerotic mice. *Pflugers Arch* 2011;462(3):371–383.
- Osei-Owusu P, Knutsen RH, Kozel BA, Dietrich HH, Blumer KJ, Mecham RP. Altered reactivity of resistance vasculature contributes to hypertension in elastin insufficiency. *Am J Physiol Heart Circ Physiol* 2014;306(5):H654–H666.

25. Measuring Cell Fluorescence Using ImageJ. 2012;2017. Available at: <https://sciencetechblog.files.wordpress.com/2011/05/measuring-cell-fluorescence-using-imagej.pdf>. Accessed [April 16, 2017].
26. Gorse KM, Lantzy MK, Lee ED, Lafrenaye AD. Transient receptor potential melastatin 4 induces astrocyte swelling but not death after diffuse traumatic brain injury. *J Neurotrauma* 2018; 35(14):1694–1704.
27. Dudenbostel T, Glasser SP. Effects of antihypertensive drugs on arterial stiffness. *Cardiol Rev* 2012;20(5):259–263.
28. Campuzano V, Segura-Puimedon M, Terrado V, et al. Reduction of NADPH-oxidase activity ameliorates the cardiovascular phenotype in a mouse model of Williams-Beuren Syndrome. *PLoS Genet* 2012;8(2):e1002458.
29. Walker AE, Henson GD, Reihl KD, et al. Greater impairments in cerebral artery compared with skeletal muscle feed artery endothelial function in a mouse model of increased large artery stiffness. *J Physiol* 2015;593(8):1931–1943.
30. Csiszar A, Lehoux S, Ungvari Z. Hemodynamic forces, vascular oxidative stress, and regulation of BMP-2/4 expression. *Antioxid Redox Signal* 2009;11(7):1683–1697.
31. Lee J, Packard RR, Hsiai TK. Blood flow modulation of vascular dynamics. *Curr Opin Lipidol* 2015;26(5):376–383.
32. Brandes RP, Weissmann N, Schröder K. Nox family NADPH oxidases in mechano-transduction: mechanisms and consequences. *Antioxid Redox Signal* 2014;20(6):887–898.
33. Chiu JJ, Chien S. Effects of disturbed flow on vascular endothelium: pathophysiological basis and clinical perspectives. *Physiol Rev* 2011;91(1):327–387.
34. Sorescu GP, Song H, Tressel SL, et al. Bone morphogenic protein 4 produced in endothelial cells by oscillatory shear stress induces monocyte adhesion by stimulating reactive oxygen species production from a nox1-based NADPH oxidase. *Circ Res* 2004;95(8):773–779.
35. Godbole AS, Lu X, Guo X, Kassab GS. NADPH oxidase has a directional response to shear stress. *Am J Physiol Heart Circ Physiol* 2009;296(1):H152–H158.
36. Van Bortel LM, Struijker-Boudier HA, Safar ME. Pulse pressure, arterial stiffness, and drug treatment of hypertension. *Hypertension* 2001;38(4):914–921.
37. Harrison DG, Gongora MC. Oxidative stress and hypertension. *Med Clin North Am* 2009;93(3):621–635.
38. Jimenez-Altayo F, Ortiz-Romero P, Puertas-Umbert L, et al. Stenosis coexists with compromised alpha1-adrenergic contractions in the ascending aorta of a mouse model of Williams-Beuren syndrome. *Sci Rep* 2020;10(1):889.
39. Wu J, Saleh MA, Kirabo A, et al. Immune activation caused by vascular oxidation promotes fibrosis and hypertension. *J Clin Invest* 2016;126(1):50–67.
40. Guzik TJ, Hoch NE, Brown KA, et al. Role of the T cell in the genesis of angiotensin II induced hypertension and vascular dysfunction. *J Exp Med* 2007;204(10):2449–2460.
41. Madhur MS, Lob HE, McCann LA, et al. Interleukin 17 promotes angiotensin II-induced hypertension and vascular dysfunction. *Hypertension* 2010;55(2):500–507.
42. Wagenseil JE, Ciliberto CH, Knutsen RH, Levy MA, Kovacs A, Mecham RP. Reduced vessel elasticity alters cardiovascular structure and function in newborn mice. *Circ Res* 2009;104(10):1217–1224.
43. Kalyanaraman B, Dranka BP, Hardy M, Michalski R, Zielonka J. HPLC-based monitoring of products formed from hydroethidine-based fluorogenic probes—the ultimate approach for intra- and extracellular superoxide detection. *Biochim Biophys Acta* 2014;1840(2):739–744.
44. Dikalov S, Griendling KK, Harrison DG. Measurement of reactive oxygen species in cardiovascular studies. *Hypertension* 2007;49(4):717–727.
45. Rastogi R, Geng X, Li F, Ding Y. NOX activation by subunit interaction and underlying mechanisms in disease. *Front Cell Neurosci* 2016;10:301.
46. Takeya R, Ueno N, Kami K, et al. Novel human homologues of p47phox and p67phox participate in activation of superoxide-producing NADPH oxidases. *J Biol Chem* 2003;278(27):25234–25246.
47. Banfi B, Clark RA, Steger K, Krause KH. Two novel proteins activate superoxide generation by the NADPH oxidase NOX1. *J Biol Chem* 2003;278(6):3510–3513.
48. Sumimoto H, Miyano K, Takeya R. Molecular composition and regulation of the Nox family NAD(P)H oxidases. *Biochem Biophys Res Commun* 2005;338(1):677–686.
49. Harrison DG, Marvar PJ, Titze JM. Vascular inflammatory cells in hypertension. *Front Physiol* 2012;3:128. doi: 10.3389/fphys.2012.00128.
50. Lee MY, San Martin A, Mehta PK, et al. Mechanisms of vascular smooth muscle NADPH oxidase 1 (Nox1) contribution to injury-induced neointimal formation. *Arterioscler Thromb Vasc Biol* 2009;29(4):480–487.
51. Troiano JA, Potje SR, Graton ME, et al. Decreased reactive oxygen species production and NOX1, NOX2, NOX4 expressions contribute to hyporeactivity to phenylephrine in aortas of pregnant SHR. *Life Sci* 2016;144:178–184.
52. Tsai MH, Jiang MJ. Reactive oxygen species are involved in regulating alpha1-adrenoceptor-activated vascular smooth muscle contraction. *J Biomed Sci* 2010;17(1):67. doi: 10.1186/1423-0127-17-67.
53. Santillo M, Colantuoni A, Mondola P, Guida B, Damiano S. NOX signaling in molecular cardiovascular mechanisms involved in the blood pressure homeostasis. *Front Physiol* 2015; 6:194. doi: 10.3389/fphys.2015.00194.
54. Craigie SM, Kant S, Keaney JF, Jr. Reactive oxygen species in endothelial function—from disease to adaptation. *Circ J* 2015; 79(6):1145–1155.
55. Gorlach A, Brandes RP, Nguyen K, Amidi M, Dehghani F, Busse R. A gp91phox containing NADPH oxidase selectively expressed in endothelial cells is a major source of oxygen radical generation in the arterial wall. *Circ Res* 2000;87(1):26–32.
56. Beckman JS, Beckman TW, Chen J, Marshall PA, Freeman BA. Apparent hydroxyl radical production by peroxynitrite: implications for endothelial injury from nitric oxide and superoxide. *Proc Natl Acad Sci USA* 1990;87(4):1620–1624.
57. Dikalova AE, Gongora MC, Harrison DG, Lambeth JD, Dikalov S, Griendling KK. Upregulation of Nox1 in vascular smooth muscle leads to impaired endothelium-dependent relaxation via eNOS uncoupling. *Am J Physiol Heart Circ Physiol* 2010; 299(3):H673–H679.
58. Walker AE, Kronquist EK, Chinen KT, et al. Cerebral and skeletal muscle feed artery vasoconstrictor responses in a mouse model with greater large elastic artery stiffness. *Exp Physiol* 2019;104(3):434–442.